Research Article | Vol. 29, No. 6 / 15 March 2021 / Optics Express 8358
Optics EXPRESS

Monolithic integration of ultraviolet light emitting diodes and photodetectors on a p-GaN/AlGaN/GaN/Si platform

QIFENG LYU, HUAXING JIANG, AND KEI MAY LAU*

Department of Electronic and Computer Engineering, Hong Kong University of Science and Technology, Hong Kong, China
*eekmlau@ust.hk

Abstract: In this letter, we report the first demonstration of monolithically integrated ultraviolet (UV) light emitting diodes (LEDs) and visible-blind UV photodetectors (PDs) employing the same p-GaN/AlGaN/GaN epi-structures grown on Si. Due to the radiative recombination of holes from the p-GaN layer with electrons from the 2-D electron gas (2DEG) accumulating at the AlGaN/GaN heterointerface, the forward biased LED with p-GaN/AlGaN/GaN junction exhibits uniform light emission at 360 nm. Facilitated by the high-mobility 2DEG channel governed by a p-GaN optical gate, the visible-blind phototransistor-type PDs show a low dark current of $\sim 10^{-7}$ mA/mm and a high responsivity of 3.5×10^5 A/W. Consequently, high-sensitivity photo response with a large photo-to-dark current ratio of over 10^6 and a response time less than 0.5 s is achieved in the PD under the UV illumination from the on-chip adjacent LED. The demonstrated simple integration scheme of high-performance UV PDs and LEDs shows great potential for various applications such as compact opto-isolators.

1. Introduction

Photonic integrated devices operating at UV spectrum can be utilized for many applications such as visible-blind light communication, bio-chemical detection and environment monitoring [1,2]. Benefitting from the direct wide bandgap material properties, GaN-based heterostructures have been widely used to build photonic devices such as light emitting diodes (LEDs) [3–6], photodetectors (PDs) [7–10] and laser diodes [11–13]. In recent years, the monolithic integration of these photonic devices to achieve multifunctional systems have drawn extensive research interests. Various approaches were employed such as the integration of LEDs and PDs sharing the same multi-quantum-well (MQW) [14–19] and the combination of high electron mobility transistors (HEMTs), LEDs and Schottky PDs with selective area epitaxy [20]. However, most of the PDs in these integration schemes showed limited responsivity and small photo-to-dark current ratio, which strongly affect the signal receiver performance such as detectivity and sensitivity. To increase the responsivity of the PDs, several structures were developed, such as avalanche photodetectors (APDs) [21–23], and transistor-type photodetectors [9,10,24–29]. Very recently, we have demonstrated a high-performance visible-blind UV PD using p-GaN/AlGaN/GaN heterostructures grown on Si, benefitting from the phototransistor-like operation mechanism [30]. In this study, taking advantage of the high-performance PD, we further demonstrate a monolithic integration of the PD with an on-chip UV light emitter employing the same p-GaN/AlGaN/GaN heterostructures. As a result, the PD exhibits a high photo-to-dark ratio of 1.5×10^6 and reasonable response time less than 0.5 s under the UV illumination from the adjacent integrated LED.

2. Heterostructure design and device fabrication

The p-GaN/AlGaN/GaN heterostructures used in this work were grown on a 6-inch Si (111) substrate by metal organic chemical vapor deposition. The epilayers, from bottom to top, consist

#418843 https://doi.org/10.1364/OE.418843
Journal © 2021 Received 30 Dec 2020; revised 4 Feb 2021; accepted 4 Feb 2021; published 2 Mar 2021

Optics EXPRESS

of a 5-μm high-resistivity GaN buffer, a 400-nm i-GaN layer, a 10-nm $Al_{0.2}Ga_{0.8}N$ barrier, and a 70-nm p-GaN cap layer with a hole concentration of ~1×10^{18} cm^{-3}. The heterostructure design is typically used for normally-OFF p-GaN gate HEMTs applications [31], which was employed here to ensure a low dark current in the PD. A 3-D schematic of the monolithically integrated devices is shown in Fig. 1. The phototransistor-like PD consists of an optical p-GaN gate (length/width=6 μm/100 μm) between two Ohmic electrodes placed on the AlGaN/GaN heterostructure. The distance between the electrodes and p-GaN is 3 μm. More information on the operation principle of the PD can be found in our previous paper [30]. Operation of the LED using the p-GaN/AlGaN/GaN heterojunction is based on radiative recombination of electrons supplied by the 2-D electron gas (2DEG) at the AlGaN/GaN heterojunction and holes from the p-GaN, under forward bias. The light emitting area of the LED is 30 μm × 100 μm, with the short side of the LED facing the PD. The cathode electrode of the LED is also 3-μm away from the p-GaN edge. The distance between LED and PD is 20 μm. The process started with p-GaN patterning to define the anode of the LED and the optical gate of the PD. The Ohmic-contact electrodes for the PD and the cathode of the LED were then formed on the exposed AlGaN barrier using an alloyed Ti/Al/Ni/Au metal stack, followed by device isolation using fluorine ion implantation. The LED and PD were thus electrically isolated with each other by the fluorine ion implantation. The resistance between the LED and PD was measured to be larger than 1 GΩ. The devices were then passivated with a 50-nm SiO_2 via plasma-enhanced chemical vapor deposition (PECVD). Transparent Ohmic-contact metal on the p-GaN of the LED part was formed using a thin Ni/Au metal stack annealed at 575°C for 5 min in nitrogen/oxygen mixture. At last, a thick pad metal of Ni/Au was deposited on the Ohmic electrodes for device measurements.

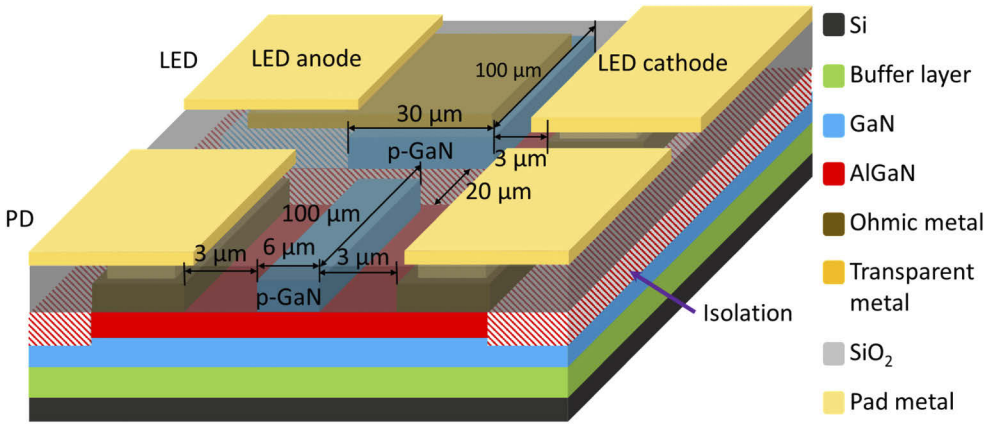

Fig. 1. 3-D schematic of the monolithically integrated LED and PD on the p-GaN/AlGaN/GaN/Si platform.

3. Results and discussions

The performance of the PD was first evaluated under the illumination of a commercial UV LED (Nichia NCSU276AT-0365) with center emission wavelength of 365 nm. Figure 2(a) compares the dark and photo current of the PD (normalized to the PD width). At 5-V bias, the PD shows a low dark current of 3.9×10^{-7} mA/mm, and a high photocurrent of 0.43 mA/mm under the UV LED illumination with an intensity of 0.024 mW/cm^2, resulting in an excellent photo-to-dark current ratio of around 1.1×10^6. The low dark current is attributed to the depletion of 2DEG at the AlGaN/GaN interface resulting in a high-resistivity channel underneath the p-GaN layer, despite a 5-V bias applied. Under UV illumination, the 2DEG channel underneath the p-GaN

Optics EXPRESS

optical gate is restored and a high Ohmic photocurrent is thus achieved [10,30]. The photocurrent and extracted responsivity of the PD as a function of the incident light intensity are shown in Fig. 2(b). An ultrahigh responsivity of 3.5×10^5 A/W is achieved in the PD. Such a large responsivity combined with the high photo-to-dark current ratio of the PD enables the device for high-sensitivity light detection on signals from the on-chip small-size LED light source even if with a relatively low output power.

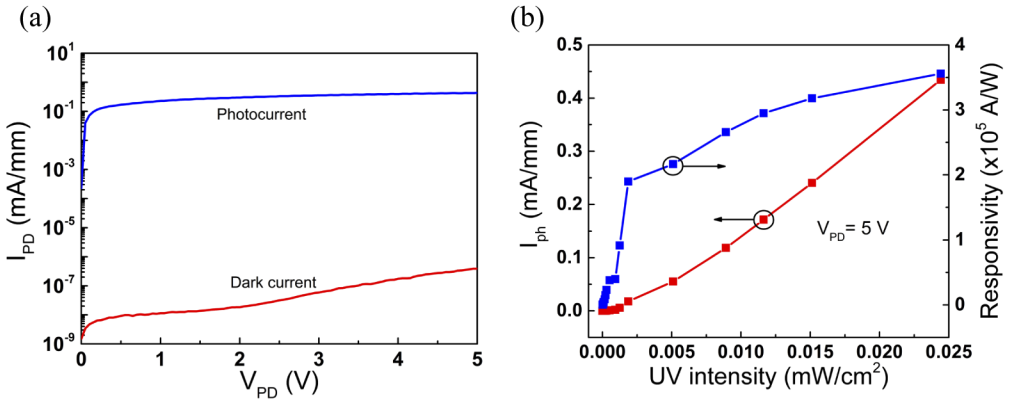

Fig. 2. (a) Dark current and photocurrent under 365-nm UV illumination of the PD. (b) Photocurrent and responsivity as a function of the UV intensity with a 5-V bias on the PD.

The forward current-voltage (I_{LED}-V_{LED}) curve of the integrated LED in linear and semi-log scale is plotted in Fig. 3(a). The device shows a relatively large turn-on voltage (V_T) of ~4.65 V, due to the depleted 2DEG in the p-GaN/AlGaN/GaN heterojunction. The operation principle of the LED can be explained as follows. When the V_{LED} is > V_T, the 2DEG restores underneath the p-GaN region. Electrons from the 2DEG and holes from the p-GaN overcome the AlGaN barrier and recombine [32,33]. Unlike conventional diode LEDs, the current saturation in the lateral access regions of the AlGaN/GaN heterostructure leads to the reduced slope in the forward *I-V* characteristics for V_{LED} > 6 V. A large I_{LED} of 267 A/cm^2 (normalized by the area of light emitting region) can be achieved at V_{LED} of 10 V, leading to uniform light emission in the p-GaN area, as shown in the inset of Fig. 3(a). Figure 3(b) shows the wavelength-dependent photo responsivity of the PD and the electroluminescence (EL) spectrum of the on-chip UV LED with different LED biases. The emission intensity of the LED as a function of wavelength was measured with a spectrometer (Ocean optics USB2000+ UV-NIR Spectrometers). The PD exhibits a cutoff wavelength of ~400 nm suggesting visible-blind operation, while the center emission wavelength of the LED is around 360 nm with a full width at half maximum of around 7 nm. The overlap of response spectrum of the PD and the emission spectrum of the LED suggests that the light emitted by the on-chip LED can be well detected by the adjacent PD.

The photo response of the PD to the UV emission from the on-chip LED is investigated as a function of bias on both the LED and PD. Figure 4(a) plots the current of the PD biased at 5 V as a function of the V_{LED}. Similar to the photo response of the PD to the external UV light source, the PD exhibits a low dark current of ~10^{-7} mA/mm before the LED turns on (for V_{LED} < 4.6 V) and a high photocurrent in the PD controlled by the LED bias is like the on/off switching of a transistor by its gate bias. Mimicking the conventional transistor operation, the current in the channel is controlled by the gate bias through the gate capacitor coupling. In our integrated system, modulation of the current in the "channel" of the PD by the spatially separated "optical gate" by the LED is realized by the transmission of UV light in the SiO_2, GaN and AlGaN between LED and PD. The V_{LED} ("gate bias") determines the LED current thereby the intensity of the emitted UV light, which then affects the photo carrier concentration

Optics EXPRESS

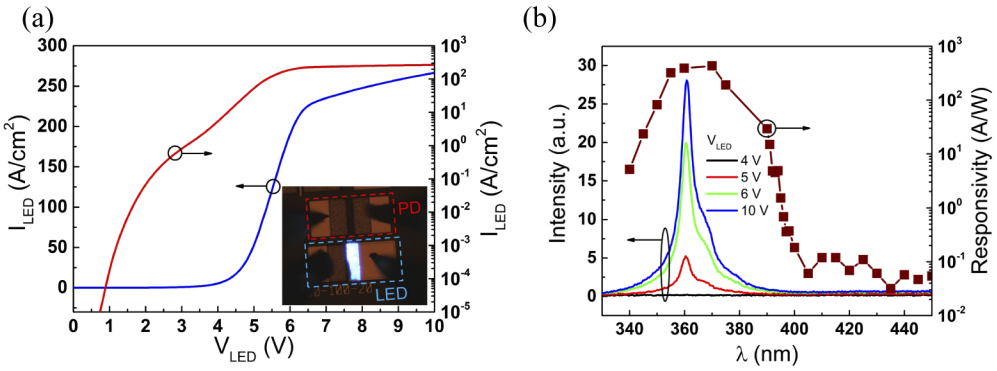

Fig. 3. (a) *I-V* curve of LED in log and linear scale. The inset is the image of the device under optical microscope when the LED is under high bias. (b) Responsivity of the PD at different wavelengths (solid-dot line) and the EL spectrum (solid line) of the on-chip UV LED with LED bias of 4 V, 5 V, 6 V and 10 V.

(conductivity) of the PD. Therefore, the integrated LED and PD together can be regarded as a fully functional transistor. Figure 4(b) shows "output" curves of the "transistor" under varying "gate" bias (corresponding to varying UV light intensity). A high maximum photocurrent of ~0.27 mA/mm is achieved in the PD at both a V_{PD} and V_{LED} of 10 V.

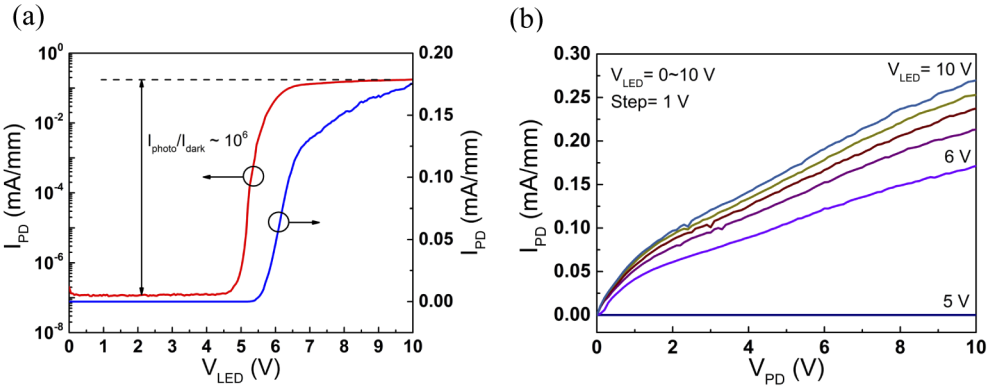

Fig. 4. (a) Photocurrent (semi-log and linear scale) of the PD at 5-V bias as a function of the LED bias. (b) Photocurrent of the PD versus the voltage drop on the PD under varying LED bias.

Figure 5 shows the photocurrent and coupling efficiency (I_{PD}/I_{LED}) at a PD bias of 5 V as a function of the LED current. A high coupling efficiency of 0.022 is derived, which is much higher than that of previous reports in literature, for instance, 1.1×10^{-6} in the Si opto-coupler [34], ~1×10^{-4} in the GaN-based integrated device [15,35,36], and ~4×10^{-3} in the AlGaN-based integrated device [17].

To evaluate the frequency response of the PD to the on-chip LED, a test platform was built with discrete and external components, as shown in Fig. 6(a). The on/off of the LED was controlled by the gate signal of a Si MOSFET, and the corresponding current in the PD was converted to a voltage signal using a resistor in series. The input gate signal of the Si transistor and the output voltage signal of the PD are presented in Fig. 6(b). The rise time (t_r) and fall time (t_f), defined as 10% to 90% of the maximum voltage, are determined to be 0.41 and 0.36 s, respectively. The RC time of the PD part of the integrated system is derived to be ~100 ns, much smaller than the rise

Optics EXPRESS

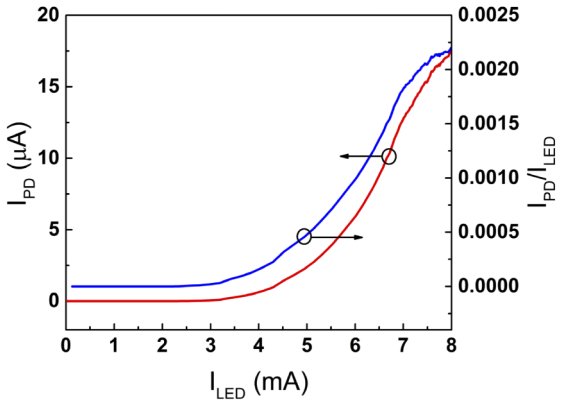

Fig. 5. Photocurrent and coupling efficiency (I_{PD}/I_{LED}) of the PD at 5-V bias as a function of the LED current

and fall time. The relatively large time constant is mainly due to a persistent photoconductivity effect in AlGaN/GaN heterostructure [37]. The longer response time of the PD in this work, compared with our previously reported device [30], may be induced by the traps in the dielectrics and the run-to-run variations in etching damage control during the p-GaN removal process. We will further optimize the p-GaN etching and surface passivation process to suppress the trapping effect thereby enabling a faster response in the PD. Applying additional gate bias on the optical p-GaN gate may also be an alternative approach to enhance the time response performance.

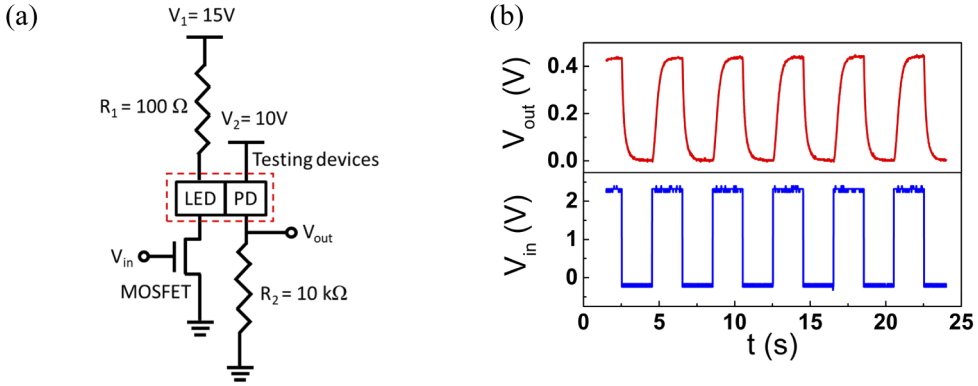

Fig. 6. (a) Circuit diagram of the frequency response test platform for the monolithically integrated UV LED and PD. (b) Waveforms of the input gate signal of the Si transistor controlling the LED and the output signal of the PD.

4. Conclusion

In conclusion, we have demonstrated a monolithically integrated UV LED and visible-blind UV PD unit, fabricated from the same p-GaN/AlGaN/GaN heterostructures grown on silicon. The UV light emitted from the LED can be well detected by the adjacent low-dark-current high-responsivity PD, with a high photo-to-dark current ratio of ~10^6. The photocurrent in the phototransistor-like PD can be effectively modulated by the forward bias of the LED, which controls the intensity of the emitted UV light. The integrated system shows a rise and fall time of 0.41 and 0.36 s, respectively. The monolithically integrated UV LEDs and PDs demonstrate

Optics EXPRESS

great potential for various applications including on-chip optical interconnect and opto-isolators working in UV regime.

Funding. Research Grants Council, University Grants Committee (16215818).

Acknowledgment. The authors thank Dr. K. Cheng from Enkris Semiconductor Inc. for providing the epi wafer and the staff of the Nanosystem Fabrication Facility (NFF) and Material Characterization and Preparation Facility (MCPF) at HKUST for their technical support.

Disclosures. The authors declare no conflicts of interest.

References

1. N. Wang, F. Tan, Y. Zhao, C. C. Tsoi, X. Fan, W. Yu, and X. Zhang, "Optofluidic UV-VIS spectrophotometer for online monitoring of photocatalytic reactions," Sci. Rep. **6**(1), 28928 (2016).
2. D. J. Blumenthal, "Photonic integration for UV to IR applications," APL Phontonics **5**(2), 020903 (2020).
3. S. Nakamura, "III-V nitride based light-emitting devices," Solid State Commun. **102**(2-3), 237–248 (1997).
4. X. Zhang, P. Li, X. Zou, J. Jiang, S. H. Yuen, C. W. Tang, and K. M. Lau, "Active matrix monolithic LED micro-display using GaN-on-Si epilayers," IEEE Photonics Technol. Lett. **31**(11), 865–868 (2019).
5. S. J. Zhou, H. H. Xu, H. P. Hu, C. Q. Gui, and S. Liu, "High quality GaN buffer layer by isoelectronic doping and its application to 365 nm InGaN/AlGaN ultraviolet light-emitting diodes," Appl. Surf. Sci. **471**, 231–238 (2019).
6. S. Y. Kuo, K. B. Hong, and T. C. Lu, "Enhanced light output of UVA GaN vertical LEDs with novel DBR mirrors," IEEE J. Quantum Electron. **51**(12), 1–5 (2015).
7. L.-H. Yang, K.-R. Lai, B.-H. Zhang, X.-L. Fu, J.-J. Wang, and W. Wei, "Polarization enhanced photoresponse of AlGaN p–i–n photodetectors," Phys. Status Solidi A **212**(3), 698–702 (2015).
8. W. Z. Xu, Y. T. Shi, F. F. Ren, D. Zhou, L. L. Su, Q. Liu, L. Cheng, J. D. Ye, D. J. Chen, R. Zhang, Y. D. Zheng, and H. Lu, "Magnesium ion-implantation-based gallium nitride p-i-n photodiode for visible-blind ultraviolet detection," Photonics Res. **7**(8), B48–B54 (2019).
9. P. F. Satterthwaite, A. S. Yalamarthy, N. A. Scandrette, A. K. M. Newaz, and D. G. Senesky, "High responsivity, low dark current ultraviolet photodetectors based on two-dimensional electron gas interdigitated transducers," ACS Photonics **5**(11), 4277–4282 (2018).
10. M. Iwaya, S. Miura, T. Fujii, S. Kamiyama, H. Amano, and I. Akasaki, "High-performance UV detector based on AlGaN/GaN junction heterostructure-field-effect transistor with a p-GaN gate," Phys. Status Solidi (c) **6**(S2), S972–S975 (2009).
11. D. B. Li, K. Jiang, X. J. Sun, and C. L. Guo, "AlGaN photonics: Recent advances in materials and ultraviolet devices," Adv. Opt. Photonics **10**(1), 43–110 (2018).
12. H.-C. Yu, Z.-W. Zheng, Y. Mei, R.-B. Xu, J.-P. Liu, H. Yang, B.-P. Zhang, T.-C. Lu, and H.-C. Kuo, "Progress and prospects of GaN-based VCSEL from near UV to green emission," Prog. Quantum Electron. **57**, 1–19 (2018).
13. T. D. Moustakas and R. Paiella, "Optoelectronic device physics and technology of nitride semiconductors from the UV to the terahertz," Rep. Prog. Phys. **80**(10), 106501 (2017).
14. W. Cai, Y. Yang, X. Gao, J. Yuan, W. Yuan, H. Zhu, and Y. Wang, "On-chip integration of suspended InGaN/GaN multiple-quantum-well devices with versatile functionalities," Opt. Express **24**(6), 6004–6010 (2016).
15. X. M. Gao, Z. Shi, Y. Jiang, S. Zhang, C. Qin, J. L. Yuan, Y. H. Liu, P. Grunberg, and Y. J. Wang, "Monolithic III-nitride photonic integration toward multifunctional devices," Opt. Lett. **42**(23), 4853–4856 (2017).
16. K. H. Li, W. Y. Fu, Y. F. Cheung, K. K. Y. Wong, Y. Wang, K. M. Lau, and H. W. Choi, "Monolithically integrated InGaN/GaN light-emitting diodes, photodetectors, and waveguides on Si substrate," Optica **5**(5), 564–569 (2018).
17. J. L. Yuan, Y. Jiang, Z. Shi, X. M. Gao, Y. J. Wang, X. J. Sun, D. B. Li, Y. H. Liu, and H. Amano, "286 nm monolithic multicomponent system," Jpn. J. Appl. Phys. **58**(1), 010909 (2019).
18. Y. C. Chiu, P. S. Yeh, T. H. Wang, T. C. Chou, C. Y. Wu, and J. J. Zhang, "An ultraviolet sensor and indicator module based on p-i-n photodiodes," Sensors **19**(22), 4938 (2019).
19. R. Floyd, K. Hussain, A. Mamun, M. Gaevski, G. Simin, M. V. S. Chandrashekhar, and A. Khan, "Photonics integrated circuits using $Al_xGa_{1-x}N$ based UVC light-emitting diodes, photodetectors and waveguides," Appl. Phys. Express **13**(2), 022003 (2020).
20. C. Liu, Y. F. Cai, H. X. Jiang, and K. M. Lau, "Monolithic integration of III-nitride voltage-controlled light emitters with dual-wavelength photodiodes by selective-area epitaxy," Opt. Lett. **43**(14), 3401–3404 (2018).
21. Z. Vashaei, E. Cicek, C. Bayram, R. McClintock, and M. Razeghi, "GaN avalanche photodiodes grown on m-plane freestanding GaN substrate," Appl. Phys. Lett. **96**(20), 201908 (2010).
22. J. Bulmer, P. Suvarna, J. Leathersich, J. Marini, I. Mahaboob, N. Newman, and F. Shahedipour-Sandvik, "Visible-blind APD heterostructure design with superior field confinement and low operating voltage," IEEE Photonics Technol. Lett. **28**(1), 39–42 (2016).
23. S. C. Shen, T. T. Kao, H. J. Kim, Y. C. Lee, J. Kim, M. H. Ji, J. H. Ryou, T. Detchprohm, and R. D. Dupuis, "GaN/InGaN avalanche phototransistors," Appl. Phys. Express **8**(3), 032101 (2015).
24. M. Martens, J. Schlegel, P. Vogt, F. Brunner, R. Lossy, J. Würfl, M. Weyers, and M. Kneissl, "High gain ultraviolet photodetectors based on AlGaN/GaN heterostructures for optical switching," Appl. Phys. Lett. **98**(21), 211114 (2011).

Optics EXPRESS

25. S. Kumar, A. S. Pratiyush, S. B. Dolmanan, S. Tripathy, R. Muralidharan, and D. N. Nath, "UV detector based on InAlN/GaN-on-Si HEMT stack with photo-to-dark current ratio > 10^7," Appl. Phys. Lett. **111**(25), 251103 (2017).
26. M. Ishiguro, K. Ikeda, M. Mizuno, M. Iwaya, T. Takeuchi, S. Kamiyama, and I. Akasaki, "Control of the detection wavelength in AlGaN/GaN-based hetero-field-effect-transistor photosensors," Jpn. J. Appl. Phys. **52**(8S), 08JF02 (2013).
27. Y. Akira, Y. Yuma, M. Takuya, I. Motoaki, T. Tetsuya, K. Satoshi, and A. Isamu, "High-photosensitivity AlGaN-based UV heterostructure-field-effect-transistor-type photosensors," Jpn. J. Appl. Phys. **55**(5S), 05FJ04 (2016).
28. L. Li, D. Hosomi, Y. Miyachi, T. Hamada, M. Miyoshi, and T. Egawa, "High-performance ultraviolet photodetectors based on lattice-matched InAlN/AlGaN heterostructure field-effect transistors gated by transparent ITO films," Appl. Phys. Lett. **111**(10), 102106 (2017).
29. P. S. Yeh, T. P. Hsu, Y. C. Chiu, S. Yang, C. Y. Wu, and J. S. Liou, "III-nitride phototransistors fabricated on a light-emitting-diode epitaxial wafer," IEEE Photonics Technol. Lett. **29**(19), 1679–1682 (2017).
30. Q. Lyu, H. Jiang, and K. M. Lau, "High gain and high ultraviolet/visible rejection ratio photodetectors using p-GaN/AlGaN/GaN heterostructures grown on Si," Appl. Phys. Lett. **117**(7), 071101 (2020).
31. H. Jiang, R. Zhu, Q. Lyu, and K. M. Lau, "High-voltage p-GaN HEMTs with off-state blocking capability after gate breakdown," IEEE Electron Device Lett. **40**(4), 530–533 (2019).
32. B. Li, H. Li, J. Wang, and X. Tang, "Asymmetric bipolar injection in a schottky-metal/ p-GaN/AlGaN/GaN device under forward bias," IEEE Electron Device Lett. **40**(9), 1389–1392 (2019).
33. X. Tang, R. Qiu, Y. Liu, and B. Li, "Thermally enhanced hole injection and breakdown in a schottky-metal/p-GaN/AlGaN/GaN device under forward bias," Appl. Phys. Lett. **117**(4), 043501 (2020).
34. V. Agarwal, S. Dutta, A. J. Annema, R. J. E. Hueting, J. Schmitz, M. J. Lee, E. Charbon, and B. Nauta, "Optocoupling in CMOS," in *2018 IEEE International Electron Devices Meeting (IEDM)* (2018).
35. Y. J. Wang, X. Wang, J. L. Yuan, X. M. Gao, and B. C. Zhu, "Monolithic III-nitride photonic circuit towards on-chip optical interconnection," Appl. Phys. Express **11**(12), 122201 (2018).
36. K. H. Li, H. T. Lu, W. Y. Fu, Y. F. Cheun, and H. W. Choi, "Intensity-stabilized LEDs with monolithically integrated photodetectors," IEEE Trans. Ind. Electron. **66**(9), 7426–7432 (2019).
37. E. Arslan, S. Bütün, S. B. Lisesivdin, M. Kasap, S. Ozcelik, and E. Ozbay, "The persistent photoconductivity effect in AlGaN/GaN heterostructures grown on sapphire and SiC substrates," J. Appl. Phys. **103**(10), 103701 (2008).